Characterization of the Structural and Surface Properties of a Synthesized Hydrous Hollandite by Gaseous Molecular Adsorption

Z.-M. Wang,*,† S. Tezuka, and H. Kanoh*,‡

Separation Technology Group, National Institute of Advanced Industrial Science and Technology, 2217-14 Hayashi-cho, Takamatsu-shi, Kagawa 761-0395, Japan

Received September 21, 2000. Revised Manuscript Received December 4, 2000

The structural and surface properties of a hydrous hollandite-type manganese oxide (H−Hol) were examined by adsorption using different gases with molecular diameters below 0.4 nm. N_2, O_2, Ar, CO, and CO_2 with diameters above 0.33 nm are excluded from the tunnel structure of H−Hol, whereas H_2O and NH_3 with diameters below 0.265 nm can be inserted into the structure. Disagreements were observed for the first and second run adsorption isotherms of H_2O and NH_3, indicating that there is a strong interaction contributing to H_2O and NH_3 adsorption. Insertion of NH_3 into the tunnels of H−Hol is a very slow process; the rate-determining step is that of insertion into the inner H^+ sites. H^+ sites on H−Hol play an important role in both NH_3 and H_2O adsorption. Adsorption and FT-IR results demonstrate that stepwise dehydration decreases the H^+ sites available for NH_3 adsorption, some but not all of which are recoverable by rehydration.

Introduction

Microporous manganese oxides are one group of crystalline transition-metal oxides containing intratunnel or layered structures whose crystalline pore dimensions are estimated to be below 1 nm. Because of their potential application in rechargeable batteries,[1−6] ion-sieving sorption,[7−12] chemical sensors,[13,14] and catalysis,[6,15−19] they have been actively studied in recent years. As one of the representative porous manganese oxides, hollandite-type manganese oxides (Hol) have a (2 × 2) tunnel structure bordered by double chains of edge-shared MnO_6 octahedra.[6,20] They can be either naturally occurring or artificially synthesized.[6] Recently, Suib et al. have extensively studied the synthesis and structural and surface properties of hollandites and Cu^{2+}-, Fe^{2+}-, and Ni^{3+}-substituting hollandites with various techniques such as X-ray diffraction (XRD), transmission electron microscopy (TEM), secondary electron microscopy (SEM), temperature-programmed desorption (TPD), and so on.[3,6,21−25] The electrochemical and ion-sieving properties of hollandites have also been widely studied for several decades.[7−9,12] However, despite great expectations as a new type of molecular sieve, research reports on its gas adsorptivity are limited. Knowledge regarding its effective pore dimension available for gas probing has not been completely proven either.

Figure 1 shows a schematic projection of hollandite structure in the (*ab*) plane. One can take a rectangular unit cell with a common size for *a* and *b*, whose edges intersect every external corner of MnO_6 octahedra surrounding the (2 × 2) tunnel.[21,22] By subtracting the thickness of the Mn layer from the interlayer space, the crystalline pore opening can be estimated as 0.46 nm. However, it is common knowledge that a crystalline pore opening is not always the same as the effective pore opening because the latter is influenced not only by

† Telephone: (+)81-87-869-3511. Fax: (+)81-87-869-3550. E-mail: zmwang@sniri.go.jp.

‡ E-mail: kano@sniri.go.jp.

(1) Kanoh, H.; Ooi, K.; Miyai, Y.; Katoh, S. *Langmuir* **1991**, *7*, 1841.
(2) Rossouw, M. H.; Liles, D. C.; Thackeray, M. M. *Mater. Res. Bull.* **1992**, *27*, 221
(3) Shen, Y. F.; Zerger, R. P.; DeGuzman, R. N.; Suib, S. L.; McCurdy, L.; Potter, D. I.; O'Young, C. L. *Science* **1993**, *260*, 511.
(4) Bach, S.; Pereira-Ramos, J. P.; Baffier, N. *Solid State Ionics* **1995**, *80*, 151.
(5) Kanoh, H.; Tang, W.; Makita, Y.; Ooi, K. *Langmuir* **1997**, *13*, 6845.
(6) Brock, S. L.; Duan, N.; Tian, Z.; Giraldo, O.; Zhou, H.; Suib, S. L. *Chem. Mater.* **1998**, *10*, 2619.
(7) Tsuji, M.; Abe, M. *Bull. Solvent Extr. Ion Exch.* **1984**, *2*, 253.
(8) Tsuji, M.; Abe, M. *Bull. Chem. Soc. Jpn.* **1985**, *58*, 1109.
(9) Clearfield, A. *Chem. Rev.* **1988**, *88*, 125.
(10) Ooi, K.; Miyai, Y.; Sakakihara, J. *Langmuir* **1991**, *7*, 1167.
(11) Tsuji, M.; Komarneni, S.; Tamura, Y.; Abe, M. *Mater. Res. Bull.* **1992**, *27*, 741.
(12) Feng, Q.; Kanoh, H.; Miyai, Y.; Ooi, K. *Chem. Mater.* **1995**, *7*, 148.
(13) Miyazaki, K.; Xu, C.-N.; Hieda, M. *J. Electrochem. Soc.* **1994**, *141*, L35.
(14) Miyazaki, K.; Hieda, M.; Kato, T. *Ind. Eng. Chem. Res.* **1997**, *36*, 88.
(15) Nitta, M. *Appl. Catal.* **1984**, *9*, 151.
(16) Cabrera, A. L.; Maple, M. B.; Arrhenius, G. *Appl. Catal.* **1990**, *64*, 309.
(17) Cao, H.; Suib, S. L. *J. Am. Chem. Soc.* **1994**, *116*, 5334.
(18) Lin, J.-C.; Chen, J.; Suib, S. L.; Cutlip, M. M.; Freihaut, J. D. *J. Catal.* **1996**, *161*, 659.
(19) Zhou, H.; Wang, J. Y.; Chen, X.; O'Young, C.-L.; Suib, S. L. *Microporous Mesoporous Mater.* **1998**, *21*, 315.
(20) Turner, S.; Buseck, P. R. *Science* **1981**, *212*, 1027.
(21) De Guzman, R. N.; Shen, Y.-F.; Shaw, B. R.; Suib, S. L.; O'Young, C.-L *Chem. Mater.* **1993**, *5*, 1395.
(22) De Guzman, R. N.; Shen, Y.-F.; Neth, E. J.; Suib, S. L.; O'Young, C.-L.; Levine, S.; Newsam, J. M. *Chem. Mater.* **1994**, *6*, 815.
(23) Wasserman, S. R.; Carrado, K. A.; Yuchs, S. E.; Shen, Y.-F.; Cao, H.; Suib, S. L. *Physica B* **1995**, *208−209*, 674.
(24) Yin, Y.-G.; Xu, W.-Q.; Suib, S. L.; O'Young, C.-L *Inorg. Chem.* **1995**, *34*, 4187.
(25) Nicolas-Tolentino, E.; Tian, Z.-R.; Zhou, H.; Xia, G.; Suib, S. L. *Chem. Mater.* **1999**, *11*, 1733.

10.1021/cm0007609 CCC: $20.00
Published on Web 01/16/2001

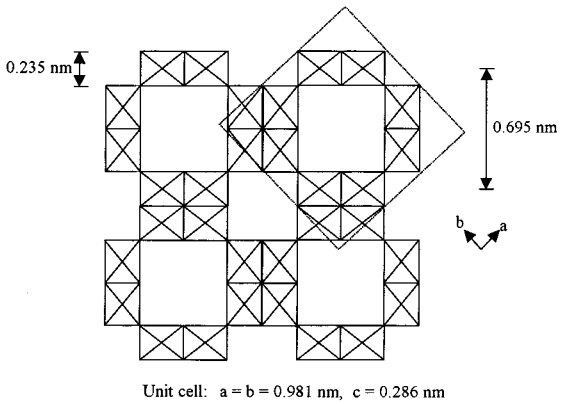

Figure 1. Projection of the (2 × 2) tunnel structure of hollandite-type manganese oxide in the (*ab*) plane.

accommodation of framework ions but also by the presence of intratunnel cations. For example, accommodation of intratunnel cations with ionic size from 0.07 (Li^+) to 0.16 nm (Cs^+)[12] in the one-dimensional tunnel of hollandite may restrict the accessibility of their tunnels to gaseous molecules. According to O'Young et al.,[26] the microporous structure of hollandite-type manganese oxides cannot be satisfactorily elucidated by low-temperature argon adsorption. The best way to probe the pore size distribution of a microporous system is the molecular probing method using gas molecules with different dimensions.[27,28] In a previous study, we reported that NH_3 can be inserted into the tunnel structure of a hydrous hollandite-type manganese oxide.[29] In the present study, we examined the micropore system of hollandite by adsorption using common molecules with molecular diameters below 0.4 nm. Emphasis has been given to adsorptivity of small NH_3 and H_2O molecules.

Experimental Section

Material and Characterization. To probe the microporous structure of Hol without the influence of cations, hydrous hollandite (H−Hol) was used in this research because the proton ionic size can be ignored. H−Hol was synthesized by the hydrothermal route reported by Thackeray et al.[2] Commercial powders of γ-MnOOH (Tosoh Co., Manganite) and Li_2CO_3 (Wako Pure Chemical Industrial Ltd., high purity) were mixed in a crucible and calcined at 1073 K for 48 h to form a Li_2MnO_3 precursor. The Li_2MnO_3 precursor was then added to a 3 M sulfuric acid solution in a Teflon-sealed autoclave, allowing hydrothermal reaction at 363 K for 48 h. The H−Hol powders produced were dried at 343 K for one night and kept in a desiccator before further use. The chemical analysis result showed that the prepared product has a unit cell chemical formula of HMn_8O_{16}; the average atomic valence for Mn is 3.88. The X-ray diffraction (XRD) pattern of the prepared H−Hol was determined by a Rigaku RINT 1200 diffractometer from 10 to 70° at a scanning speed of 0.02°/min in a chamber with humidity and temperature control. The thermal gravimetry (TG) and differential thermal analysis (DTA) of the prepared H−Hol were carried out with a TG-DTA 2000 system (Mac Science Co. Ltd.) at a ramp rate of 10 K/min. Commercial α-Al_2O_3 was used as a standard material for TG/DTA measurements.

Adsorption Measurement. The adsorption of N_2, O_2, Ar, CO, CO_2, H_2O, and NH_3 was carried out by a volumetric method using commercial volumetric apparatus (Autosorp-1 of Quanta-Chrom Co. or Belsorp 18 of Japan Bell Co.). The adsorption temperatures are 77 K for N_2, O_2, Ar, and CO, 195 K for CO_2, and a temperature in the range of 278−318 K for H_2O and NH_3. Prior to adsorption, the samples were evacuated under 1 mPa at 393 K (or 573 K) for 2 h. After completion of a first-run adsorption, H_2O or NH_3-adsorbed H−Hol was evacuated under 10 mPa at the adsorption temperature for at least 2 h and then subjected to a second-run adsorption at the same temperature. The amount of irreversible NH_3 and H_2O adsorption was obtained by subtracting the second-run adsorption isotherm from the first. The relationship of H_2O and NH_3 adsorption on H−Hol to pre-evacuation temperature (393, 473, or 573 K) was also examined. The NH_3 or H_2O adsorption on H_2O- or NH_3-preadsorbed H−Hol was carried out after evacuating the sample preadsorbed by H_2O for 2 h or NH_3 for 30 min at the same adsorption temperature. The equilibrium time for obtaining every point of adsorption isotherm is 300 s for NH_3 and 500 s for the other gases. Commercial gases with purities greater than 99.99% were used for adsorption measurements without further purification. H_2O was purified by the freeze−pump−thaw method before use.

FT-IR Spectroscopic Measurement. The NH_3 surface adspecies and the change of surface sites on H−Hol for NH_3 adsorption were observed by FT-IR spectroscopy. A special quartz cell mounted with a pair of NaCl windows to allow penetration of an IR beam through the centers of the windows was connected to a vacuum line for sample pre-evacuation and introduction of gas without exposure to the atmosphere. Prior to measurements, H−Hol was pressed at 250 kPa to form a thin wafer of 1 cm diameter, which was placed in a quartz holder suspended by means of a Pt wire in the quartz cell. After evacuation at 393 K for 15 min (condition a) at the upper part of quartz cell, the H−Hol wafer was shifted down to the measurement position in a room temperature environment (295−297 K). NH_3 was then introduced and maintained at equilibrium pressures of 1.0 (condition b) and 3.6 kPa (condition c) for 15 min each. After the NH_3-adsorbed H−Hol was successively evacuated at 393 (condition d) and 473 K (condition e) for 15 min each, the sample was subjected to another NH_3 adsorption at an equilibrium pressure of 3.2 kPa for 15 min (condition f) and then evacuated at 473 (condition g) and 573 K (condition h), for 15 min each. After that, NH_3 adsorption at room temperature and desorption at 573 K were repeated four times with an NH_3 equilibrium pressure of 1.6, 1.1, 1.2, or 1.0 kPa and at an adsorption time of 15 min each (Conditions i, j, k, l, m, n, o, and p sequentially represent each of the adsorption and desorption steps). Finally, the sample was evacuated at 573 K for 25 min (condition q), and at 773 (condition r) and 973 K (condition s) for 10 min each. The IR absorbance corresponding to each of the above steps was collected from 32 scans at a resolution of 2 cm^{-1}. NH_3 gas of 99.999% purity was used for IR measurements after further purification by a freeze−pump−thaw method.

Results and Discussion

Sample Characterization and Adsorption of Various Gaseous Molecules on H−Hol. XRD measurements confirm that the prepared H−Hol has a structure similar to natural cryptomelane,[30,31] having a tetragonal unit cell of $a = b = 0.981$ nm and $c = 0.286$ nm (Figure 1). Figure 2 shows the change in XRD patterns of the prepared H−Hol after evacuation at

(26) O'Young, C.-L.; Sawicki, R. A.; Suib, S. L. *Microporous Mater.* **1997**, *11*, 1.
(27) Gregg, S. J.; Sing, K. S. W. *Adsorption, Surface Area and Porosity*; Academic Press: London, 1982.
(28) Rouquerol, F.; Rouquerol, J.; Sing, K. S. W. *Adsorption by Powders & Porous Solid*; Academic Press: San Diego, 1999.
(29) Tezuka, S.; Wang, Z.-M.; Ooi, K.; Kanoh, H. *Adsorption Science, & Technology*; Do, D. D., Ed.; World Scientific: Singapore, 2000; pp 319−323.
(30) JCPDS-ICDD Powder Diffraction File No. 20-908.
(31) Burns, R. G.; Burns, V. M. *Manganese Dioxide Symposium*; Schumm, B., Jr., Joseph, H. M., Kozawa, A., Eds.; I. C. MnO_2 Sample Office: Cleveland, 1981; pp 97−112.

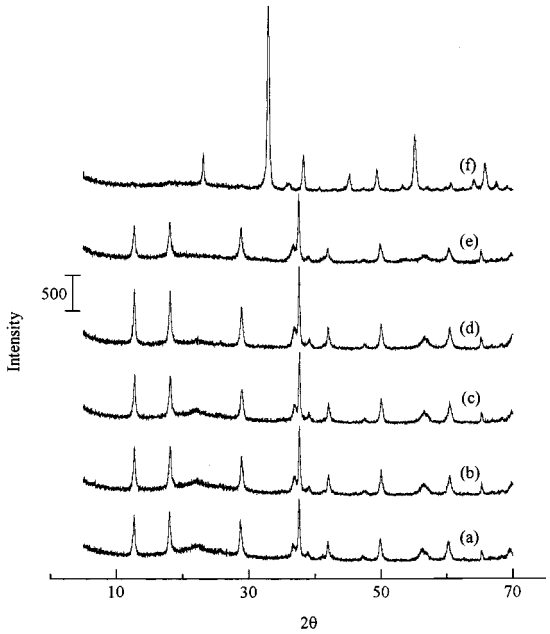

Figure 2. XRD patterns of (a) as-prepared H−Hol and those after evacuation for 2 h at (b) 373, (c) 473, (d) 573, (e) 673, and (f) 773 K.

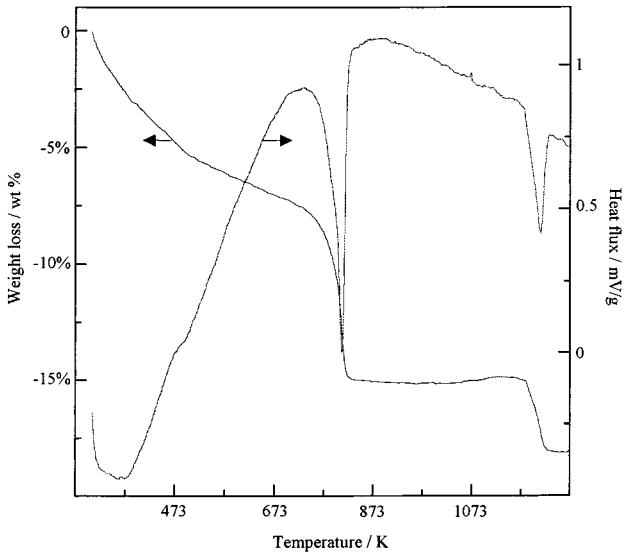

Figure 3. TG/DTA curves of the as-prepared H−Hol. Condition: ramp rate, 10 K/min; curtain gas, air (100 mL/min).

various temperatures for 2 h. The prepared H−Hol basically resists temperature-induced changes up to and including 673 K although the diffraction peaks were broader and of less intensity with evacuation at 673 K. Dehydration at 773 K leads to the transformation of hollandite to an α-Mn_2O_3 crystal. The TG/DTA curves of the as-prepared H−Hol in Figure 3 show the result corresponding to the XRD pattern changes in Figure 2, giving a gradual dehydration until 673 K before the first endothermic peak due to the crystal transformation to α-Mn_2O_3. The second crystal transformation from α-Mn_2O_3 to Mn_3O_4 gives rise to a second step in the TG curve and a great endothermic peak in the DTA curve at around 1200 K. The extent of dehydration, 6.2 wt %, between 303 and 673 K is much greater than that released by detachment of the H^+ contents in H−Hol (∼1.3 wt %), indicating that one part of water can be

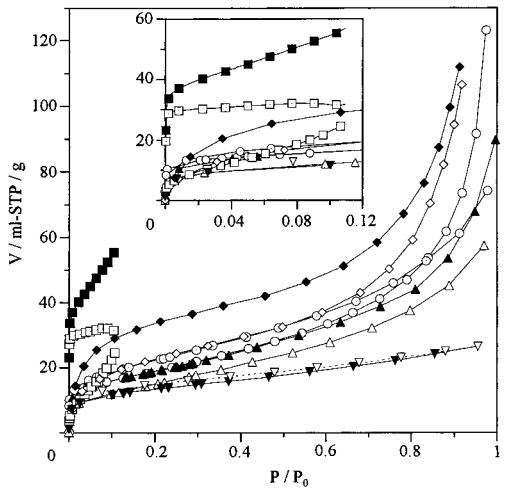

Figure 4. Adsorption isotherms of N_2 (○), O_2 (⊙), Ar (▲), and CO (△) at 77 K, CO_2 (▼) at 195 K, NH_3 first run (■), NH_3 second run (□), and the difference between first and second runs (⊡) at 298 K, and H_2O first (◆) and second (◇) runs at 298 K, and CO_2 desorption isotherm at 195 K (▽).

retained on the surface of H−Hol until high temperature.

Figure 4 shows the adsorption isotherms of Ar and CO in comparison with those of N_2 and O_2 at 77 K, CO_2 adsorption isotherm at 195 K, the first- and second-run adsorption isotherms of H_2O and NH_3 at 298 K, and an irreversible adsorption isotherm of NH_3 at 298 K on H−Hol. All the adsorption isotherms except that of NH_3 show typical type II shapes, which are characteristic of multilayer condensation on a flat surface.[27] No hysteresis was observed in the desorption branches of Ar, CO, N_2, and O_2 (not shown for clarity), indicating that no mesopores were present as probed by these molecules in H−Hol. However, a slight desorption hysteresis became evident for CO_2 having a smaller molecular diameter (0.33 nm[37]). This desorption hysteresis persists to the lower P/P_0 value ($P/P_0 < 0.1$), demonstrating the existence of activated adsorption and stronger inclusion of CO_2 in the micropores of H−Hol. The first-run adsorption isotherm of NH_3 showed a sharp uprising at $P/P_0 < 0.01$ and a gradual increase after $P/P_0 = 0.01$. The sequence of adsorption amount at $P/P_0 = 0.3$ on H−Hol is NH_3 (first-run) > H_2O (first-run) > O_2 > N_2 = Ar > CO = CO_2. NH_3 and H_2O adsorption amounts are 2−3-fold greater than those of other gases. The disagreement between the first- and the second-run adsorption of NH_3 and H_2O implies the existence of a strong interaction of NH_3 and H_2O with the surface of H−Hol. Formation of NH_4^+ by NH_3 adsorption[29] leads to a greatly enhanced irreversible adsorption at low relative pressure. A comparatively slight irreversible H_2O adsorption is ascribed to either the stronger H-bond interaction or the possible formation of H_3O^+ species, which have been confirmed from the lattice expansion phenomenon of H−Hol after H_2O adsorption by XRD measurements. To make parallel comparisons, the Brunauer−Emmett−Teller (BET) equation was applied for all isotherms to calculate the specific surface areas, S_{BET}, despite possible involvement of chemisorption in case of NH_3 and H_2O. As shown in Table 1, the S_{BET} values from Ar, CO, CO_2, N_2, and O_2 adsorption are very similar to one another but smaller or much smaller than

Table 1. Surface Area of H−Hol Calculated from Adsorption of Each Gas

adsorbate	evacuation *T*/K	*d*/nm	adsorption *T*/K	S_{BET}/m²/g	$S_{t,total}$[a]/m²/g	$S_{t,ext}$[a]/m²/g	$S_{t,int}$[a]/m²/g
N_2	393	0.364	77	73	68	56	12
	573		77	79			
O_2	573	0.346	77	71	nd	nd	nd
Ar	573	0.340	77	79	nd	nd	nd
CO	573	0.376	77	67	nd	nd	nd
CO_2	573	0.330	195	64	nd	nd	nd
H_2O (first run)	393	0.265	298	95	nd	nd	nd
NH_3 (first run)	393	0.26	298	161	nd	nd	nd

[a] nd: Not determined.

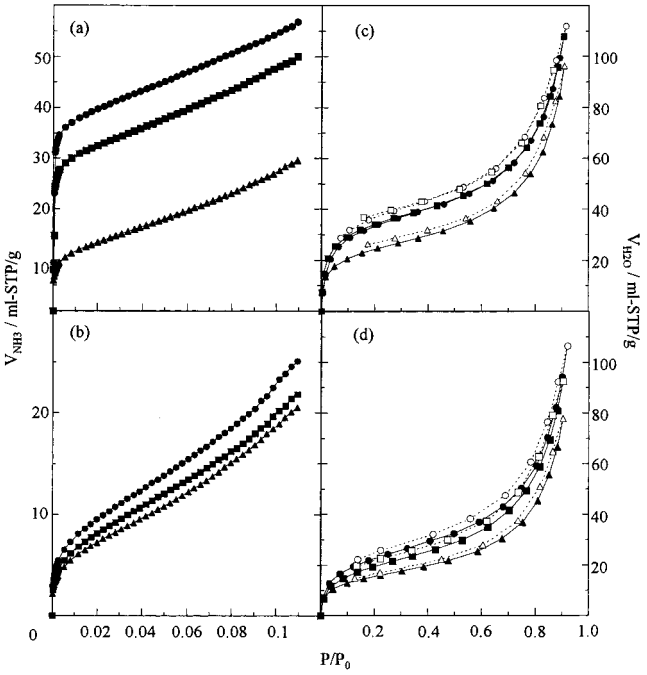

Figure 5. (a) First- and (b) second-run NH_3 adsorption isotherms and (c) first- and (d) second-run H_2O adsorption isotherms on H−Hol at 298 K after preevacuation at 393 (●), 473 (■), and 573 K (▲). Unfilled symbols represent the desorption branch of the adsorption with the same type of symbol.

those from H_2O (first-run) or NH_3 (first-run) adsorption. By analyzing the adsorption isotherms using a de Boer *t*-plot,[32] it is possible to know the internal and external surface areas. On the basis of a standard N_2 adsorption isotherm on nonporous alumina,[27,32] we obtained from the N_2 adsorption isotherm the total, the external, and the internal surface areas, denoted as $S_{t,total}$, $S_{t,ext}$, $S_{t,int}$, respectively. As shown in Table 1, the $S_{t,ext}$ values from N_2 adsorption are very close to those of $S_{t,total}$ and S_{BET} values. It thus follows that not only N_2 but also O_2, Ar, CO, and CO_2 are excluded from the microporous tunnels of H−Hol. The greater S_{BET} values from NH_3 and H_2O adsorption demonstrate that the two molecules can be inserted into the tunnel structure although it is hard for the inserted NH_3 and H_2O to be desorbed because of strong localization. Although H−Hol has a crystalline pore opening of 0.46 nm, its effective pore opening must be less than 0.33 nm (the dynamic diameter, *d*, of CO_2[37]) and close to 0.265 nm (the *d* value of H_2O[37]).

Relationship of NH_3 and H_2O Adsorption with the Extent of Dehydration of H−Hol. Figure 5 shows the first- and second-run adsorption isotherms of NH_3 and H_2O at 298 K on H−Hol after dehydration at various temperatures. Both the first- and second-run adsorption amounts of NH_3 decreased with increase of dehydration temperature, demonstrating that H^+ content in H−Hol plays an important role in NH_3 adsorption. The smaller difference among the second-run adsorption amounts of NH_3 at various dehydration temperatures indicates that protons contained in H−Hol have a great responsibility for irreversible NH_3 adsorption. Table 2 shows the NH_3 adsorption amounts at 298 K on H−Hol (at $P/P_0 = 0.027$), $V_{NH3,s}$, at various dehydration temperatures. The NH_3 irreversible adsorption amount on H−Hol at a dehydration temperature of 573 K is less than one-fourth of that at a dehydration temperature of 393 K. Since it is not easy to apply an adsorption theory to analysis of NH_3 adsorption isotherms, which contain contributions from both chemisorption and physical adsorption, we only fit the irreversible NH_3 adsorption isotherms with the Langmuir equation (not shown for clarity), whereas the surface area for irreversible NH_3 adsorption, S_{irr}, was calculated from the Langmuir saturated adsorption amount by tentatively using the NH_3 molecular sectional area (0.129 nm²).[33] As shown in Table 2, the Langmuir saturated adsorption amount of NH_3 matches well with $V_{NH3,s}$. The S_{irr} values at dehydration temperatures of 393 and 473 K are much greater than the S_{BET} values from Ar, N_2, O_2, CO, and CO_2 adsorption, revealing a great contribution of chemisorption during NH_3 adsorption.

Table 2. NH_3 Adsorption Amount at $P/P_0 = 0.027$, $V_{NH_3,s}$, and Irreversible Surface Area, S_{irr}, under Various Conditions

		$V_{NH_3,s}$/mL-STP/g			
evacuation *T*/K	adsorption *T*/K	first-run	second-run	irrev. (Langmuir)	S_{irr} m²/g
393	278	40	13	27 (27)	91
	298	41	11	30 (31)	104
	318	42	13	29 (34)	114
473	278	29	12	17 (18)	60
	298	34	9	25 (25)	84
	298[a]	38	13	25 (25)	[b]
	318	35	11	24 (24)	81
573	278	16	9	7 (7)	24
	298	15	8	7 (6)	20
	298[a]	26	10	16 (16)	[b]
	318	16	8	8 (7)	25

[a] After H_2O preadsorption. [b] Not determined.

On the other hand, while the first-run adsorption isotherms of H_2O for dehydration at 393 and 473 K overlap with each other, the second-run adsorption for

(32) Lippens, B. C.; de Boer, J. H. *J. Catal.* **1965**, *4*, 319.

(33) Young, D. M.; Crowell, A. D. *The Physical Adsorption of Gases*; Butterworth : London, 1962.

Table 3. H_2O Adsorption Area under Various Conditions

evacuation *T*/K	adsorption *T*/K	$S_{BET,H_2O}/m^2/g$ first-run	second-run	irrev.
393	283	71	53	17
	298	91	61	30
	298[a]	50	[b]	[b]
	308	100	73	26
473	298	92	55	37
	298[a]	55	[b]	[b]
573	283	74	46	28
	298	68	44	23
	308	75	48	26

[a] After NH_3 preadsorption. [b] Not determined.

dehydration at 473 K is slightly smaller than that for dehydration at 393 K, indicating that the dehydrated sites at 473 K are recoverable on readsorption of H_2O possibly due to dissociative adsorption. In contrast to the case of NH_3 adsorption, the reduction in the first-run H_2O adsorption amount between dehydration temperatures of 393 and 573 K is almost the same as that in the second-run adsorption amount, indicating that high-temperature dehydration has a smaller effect on the reduction of irreversible adsorption of H_2O. Table 3 shows the S_{BET,H_2O} values from H_2O adsorption at 298 K after dehydration at various temperatures. The S_{BET,H_2O} values from the second-run H_2O adsorption isotherms at dehydration temperatures of 573 K are even smaller than the $S_{t,ext}$ values from N_2 adsorption, reflecting the important role of surface H^+ sites on H−Hol in H_2O adsorption. Since the crystal structure is not greatly changed by dehydration until 673 K, as shown by the XRD result, the tunnel porous structure of H−Hol may not significantly change until 673 K. The small H_2O adsorption at the dehydration temperature of 573 K implies the disappearance of H_2O dissociative adsorption sites due to a partial rearrangement of the H−Hol surface by certain valence transformation of surface Mn ions (Mn(IV) → Mn(III)).

Figure 6 shows the NH_3 and H_2O adsorption isotherms at 298 K on H_2O- and NH_3-preadsorbed H−Hol, respectively. Preadsorption of H_2O on H−Hol dehydrated at 473 K slightly enhanced the weak NH_3 adsorption, leading to the second-run NH_3 adsorption amount which is the same as that at dehydration temperatures of 393 K, but had almost no effect on irreversible NH_3 adsorption. This result correlates with the above results, in which dehydration at 473 K leads to detachment of one part of weak H^+ sites on H−Hol, which can be reversibly recovered. Readsorption of H_2O produces weak H^+ sites by dissociative adsorption for NH_3 adsorption, whereas one part of the strong H^+ sites is irreversibly lost by surface rearrangements due to Mn ion valence changes at dehydration temperatures of 473 K. On the other hand, preadsorption of H_2O on H−Hol dehydrated at 573 K did not increase the weak NH_3 adsorption (the second-run adsorption) while largely enhancing the irreversible NH_3 adsorption, indicating that, by dehydration at 573 K, the weak H^+ sites disappear by surface rearrangements while one part of the dehydrated sites from strong H^+ sites can still be recovered by readsorption of H_2O. In addition, the amount of irreversible NH_3 adsorption on H_2O-preadsorbed H−Hol after dehydration at 573 K is still smaller than that on H−Hol dehydrated at 473 K, implying that one part of the strong NH_3 adsorption sites is also irreversibly lost by

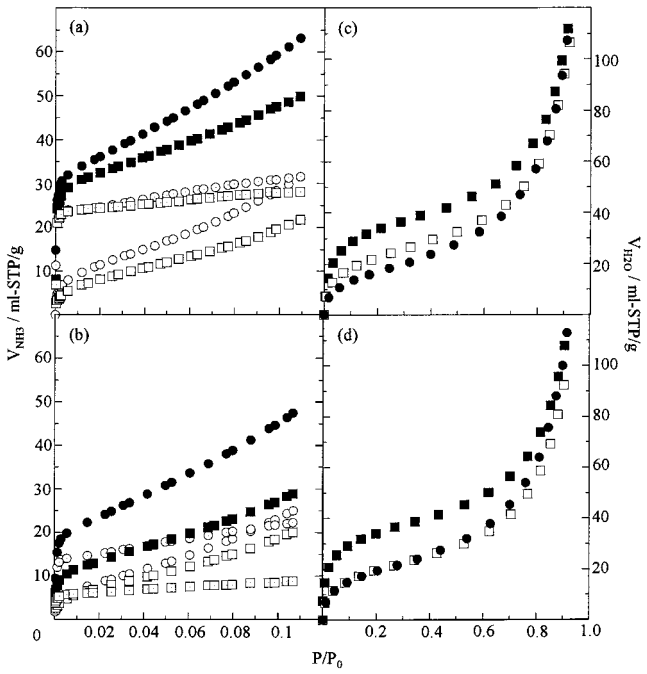

Figure 6. Comparison of NH_3 adsorption isotherms at 298 K on fresh and H_2O preadsorbed H−Hol after evacuation at (a) 473 and (b) 573 K, respectively, and those of H_2O at 298 K on fresh and NH_3 preadsorbed H−Hol after evacuation at (c) 393 and (d) 473 K, respectively. ■, □, ⊡: first-run, second-run, and irreversible adsorption without H_2O or NH_3 preadsorption, respectively. ●, ○, ⊙: first-run, second-run, and irreversible adsorption with H_2O or NH_3 preadsorption, respectively.

dehydration at 573 K. When NH_3 was preadsorbed on H−Hol dehydrated at 393 K, the H_2O adsorption amount was smaller than that of the second-run adsorption without NH_3 preadsorption. This decrease in H_2O adsorption is ascribed to NH_3 occupying weak H^+ sites, which will be lost by dehydration at 473 K and is reproducible by H_2O readsorption, because the decrease in the second-run H_2O adsorption by NH_3 preadsorption on H−Hol dehydrated at 393 K (11 m^2/g from Table 3) is similar to twice the difference of S_{BET,H_2O} from the second-run H_2O adsorption at dehydration temperatures between 393 and 473 K (6 m^2/g from Table 3). However, the H_2O adsorption isotherm on H−Hol preadsorbed by NH_3 overlaps very well with the second-run H_2O adsorption without NH_3 preadsorption on H−Hol dehydrated at 473 K. This phenomenon suggests that H_2O cannot be inserted into the innermost H^+ sites in the tunnel where NH_3 can be strongly adsorbed.

Relationship of NH_3 and H_2O Adsorption with Adsorption Temperature. Figure 7 shows NH_3 and H_2O adsorption isotherms on H−Hol at various adsorption temperatures. Increasing the adsorption temperature in the range of 278−318 K gradually increased not only the first-run but also the second-run NH_3 adsorption, indicating that even second-run NH_3 adsorption is partially specific. Calorimetric results show that the initial second-run NH_3 adsorption heat can be as high as 80−90 kJ/mol,[34] much more than the condensation heat of NH_3 (19.9 kJ/mol at 298 K[35]), reflecting its property of specific adsorption. On the other hand, while

(34) Wang, Z.-M.; Kanoh, H. unpublished results.
(35) *Handbook of Chemistry and Physics*, 76th ed.; David, R. L., Ed.; CRC Press: Boca Raton, 1995; pp 6−116.

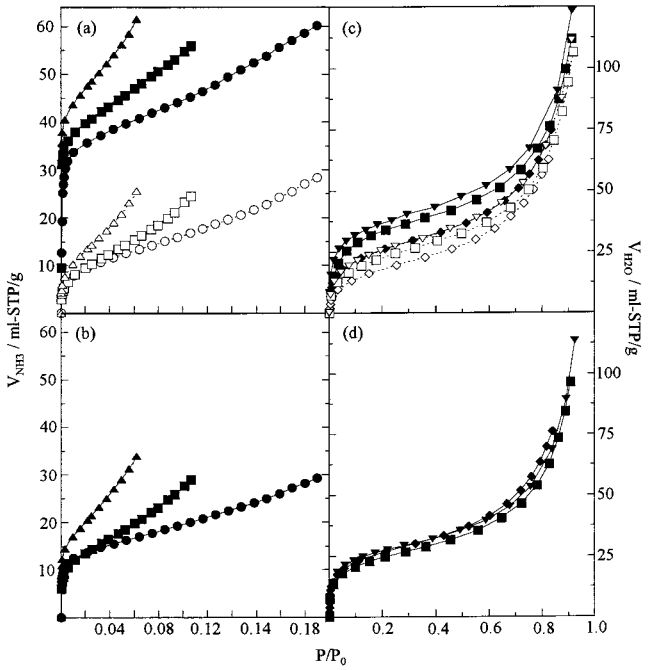

Figure 7. Adsorption isotherms for NH_3 at 278 (●, ○), 298 (■, □), and 318 K (▲, △) and those for H_2O at 283 (◆, ◇), 298 (■, □), and 308 (▼, ▽) K on H−Hol after evacuation at (a) 473 and (b) 573 K for NH_3 and (c) 473 and (d) 573 K for H_2O. The solid and unfilled symbols represent first- and second-run adsorption, respectively.

the same specific properties of the first- and second-run H_2O adsorption were observed on H−Hol dehydrated at 473 K, the H_2O adsorption on H−Hol dehydrated at 573 K did not change significantly with adsorption temperature. This result coincides with those in the above section, further indicating that weak H^+ sites disappear by dehydration at 573 K and that the innermost strong H^+ sites are not accessible to H_2O adsorption.

As shown in Tables 2 and 3, the irreversible adsorption of NH_3 and H_2O basically increased with increase of adsorption temperature, indicating that adsorption of NH_3 or H_2O may be controlled by an activation adsorption to expand the lattice structure due to formation of larger NH_4^+ or H_3O^+ as well as diffusion resistance along the tunnel pore structure. Figure 8 shows the time-courses of first-run NH_3 adsorption at 283 and 298 K on H−Hol dehydrated at 393 K. A common adsorption rate was observed at the initial adsorption stages (t < 100 s) for the two adsorption temperatures. However, a difference in adsorption rate became apparent after t = 100 s. The higher adsorption temperature accelerates NH_3 adsorption, resulting in a higher adsorption amount with time. The change in the time course of NH_3 indicates that two sub-stages exist for NH_3 adsorption on H−Hol: one is the initial stage occurring at the external surface or near the entrance, and the other is the NH_3 insertion stage into the intratunnel structure, which is the more rate-determining process.

FT-IR Observation of NH_3 Adsorption Sites on Repeated Adsorption−Desorption Cycling. Figure 9 shows the NH_3 adspecies in the range around 1400 cm^{-1} under various conditions (the detailed description on the conditions is given in the Experimental Section).

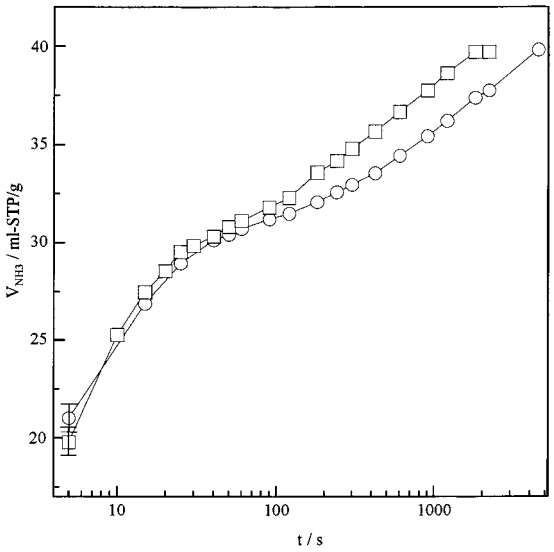

Figure 8. Time-courses of first-run NH_3 adsorptions at 283 (○) and 298 (□) K with Pe = 2 kPa on H−Hol dehydrated at 393 K.

After evacuation of H−Hol at 393 K (condition a), a small sharp peak at 1420 cm^{-1} was observed. Because this band always appeared after the same procedure for several different batches of H−Hol samples, we suppose that it came from some contaminants, e.g., some adsorbed NH_4^+ species or other adspecies. NH_3 adsorption on H−Hol dehydrated at 393 K (condition b) gave a sharp peak of great intensity at 1400 cm^{-1}, which can be ascribed to an NH_4^+ species.[36] This peak was not seriously enhanced by rising NH_3 gas pressure (condition c) but gradually decreased by evacuation at 393 and 473 K (conditions d and e). The position of NH_4^+ species was constant after desorption at 393 K but shifted to a higher band position after that at 473 K. NH_3 readsorption (condition f) on H−Hol successively evacuated at 473 K again gave a sharp peak at 1400 cm^{-1} and subsequent desorption (condition g) at 473 K retained the same peak shapes and positions as that of condition e. Thus, NH_3 adsorption sites to form NH_4^+ species are not changed and NH_3 can be repeatedly adsorbed on H−Hol at a dehydration temperature below 473 K although the irreversible NH_3 adspecies cannot be completely desorbed. However, NH_3 adsorption on H−Hol successively evacuated at 573 K leads to only a slight increase in the peak at 1420 cm^{-1} instead of a peak at 1400 cm^{-1} (condition i). A peak at 1600 cm^{-1}, which can be assigned to an NH_3 adspecies on Lewis acid sites,[36] also concurrently appeared. With the increase in the number of repeated cycling of NH_3 adsorption−desorption (at 573 K), the peak at 1420 cm^{-1} gradually decreased in intensity in concurrence with the gradual increase in intensity of the peak at 1600 cm^{-1} and finally disappeared (conditions j−p). Thus, the change in NH_3 adsorption sites on repeated adsorption−desorption (at 573 K) reflects the gradual diminishing of H^+ sites on H−Hol and their transformation to Lewis acid sites, suggesting easy rearrangement of the H−Hol surface at a dehydration temperature of 573 K. The appearance of two $-NH_4^+$ adspecies implies the pres-

(36) Tsyganenko, A. A.; Pozdnyakov, D. V.; Filimonov, V. N. *J. Mol. Struct.* **1975**, *29*, 299.

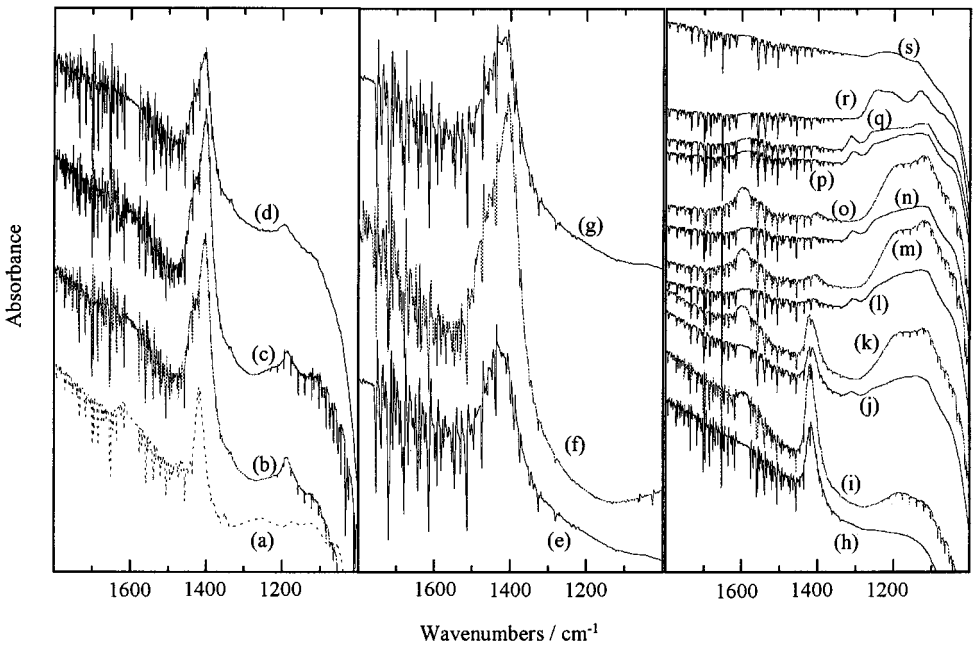

Figure 9. FT-IR observation on repeating NH_3 adsorption−vacuum evacuation. Conditions (a−s) are the same as those described in the Experimental Section.

ence of two NH_3 adsorption sites on H−Hol: the comparatively weak H^+ sites exist in large amounts but disappear on evacuation above 573 K, and the stronger, less plentiful H^+ sites can be retained at a higher temperature. As the result of sufficient dehydration, surface rearrangement, and partial or complete destruction of the hollandite structure, the NH_3 adsorption sites are almost entirely lost and NH_3 adspecies become obscure by evacuation above 673 K (conditions q to s).

Schematic Model for the Structural and Surface Properties of H−Hol and Their Changes on Increasing Temperature. From the above adsorption results, a schematic model of the pore structure of H−Hol for gas adsorption is shown in Figure 10a. Although the crystalline pore opening of H−Hol is estimated as 0.46 nm,[21,22] we believe that this pore opening is the distance between the centers of oxygen ions of the two neighboring MnO_6 octahedra on each side of the (2 × 2) tunnel. The dimension of 0.216 nm obtained by subtracting the diameter of O^{2-} ions (0.244 nm for a three coordination number[35]) from 0.46 nm is small enough to exclude Ar, N_2, O_2, CO, and CO_2 with dynamic molecular diameters between 0.33−0.364 nm[37] from the tunnel. Although the value of 0.216 nm depends on the O^{2-} radius value in the literature, it is rather close to the dynamic diameters of H_2O and NH_3 (H_2O, 0.265 nm; NH_3, 0.26 nm[37]). This may explain why adsorption, especially physical adsorption of H_2O and NH_3, into the tunnel is not easy but requires the aid of stronger irreversible adsorption. Hence, adsorption isotherms for NH_3 and H_2O previously shown may not reflect a real equilibrium adsorption but a quasi-equilibrium adsorption. The difference in H_2O and NH_3 adsorption can be ascribed either to a thermodynamic disadvantage due to the weaker specific interaction or a higher activation energy to form H_3O^+ than to form NH_4^+ or to a larger diffusion resistance along the tunnel

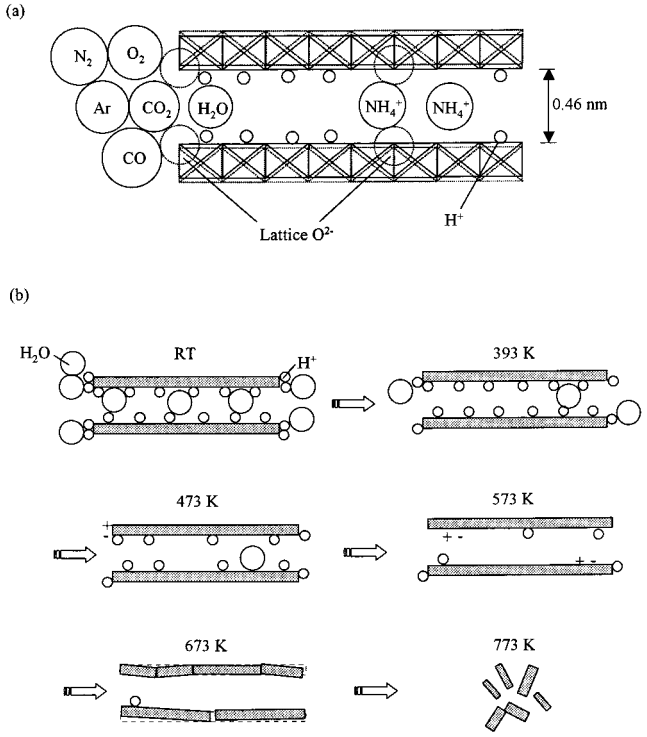

Figure 10. (a) Molecular adsorption schematic of N_2, O_2, Ar, CO, CO_2, H_2O, and NH_3 on H−Hol and (b) dehydration schematic of H−Hol with increasing temperature.

structure due to a larger molecular size of H_2O in comparison with NH_3. Strong acid−base interactions give NH_3 molecules great accessibility to the innermost H^+ sites with strong adsorption energy. Formation of NH_4^+ due to NH_3 adsorption brings about expansion of the lattice structure,[29] leading to NH_3 being more easily transported along the one-dimensional tunnel.

Figure 10b shows a schematic model describing the dehydration process of H−Hol. As the dehydration amount of H−Hol from room temperature to 673 K is much larger than the theoretical H_2O amount from the

(37) Breck, D. W. *Zeolite Molecular Sieves − Structure, Chemistry, and Use*; Wiley-Interscience: New York, 1974.

lattice protons, it seems from the H_2O and NH_3 adsorption results that lattice protons desorb sequentially from weaker to stronger intensity protons together with included water. Dehydration of H−Hol is unlike that in other metal oxides such as silica, alumina, and so on, which lose their physisorbed H_2O first and then surface hydroxy groups next with increasing temperature. Under the mild dehydration condition at 393 K, most of the water is desorbed, leaving the largest amount of exposed H^+ on H−Hol, on which the largest amount of NH_3 can be adsorbed irreversibly. By dehydration at 473 K, detachment of water and external H^+ sites becomes sufficient to give rise to some coordinately unsaturated (cus) sites on the external surface of H−Hol, which can then serve as new dissociative sites for water adsorption. Dehydration at 573 K leads to rearrangement of surface sites on the external surface, namely, the disappearance of cus sites at the external surface while producing some cus sites inside the tunnel structure. The cus sites near the entrance will then be dissociative sites for H_2O adsorption and NH_3 adsorption sites after rehydration. Finally, dehydration above 673 K leads to sufficient disappearance of lattice protons and partial or complete collapse of the crystal structure, thus bringing about minimal NH_3 adsorption.

Conclusion

1. Adsorption results show that N_2, O_2, Ar, CO, and CO_2 with molecular diameters above 0.33 nm are excluded from the tunnel structure of H−Hol. However, H_2O and NH_3 can be inserted into the tunnel structure with the aid of strong interaction with the surface of H−Hol. These results indicate that the effective pore opening of H−Hol for gas adsorption is around 0.265 nm, i.e., the molecular diameter of H_2O.

2. Dehydration decreases not only the adsorption amount of NH_3 but also that of H_2O, indicating that H^+ contents in H−Hol play an important role in both NH_3 and H_2O adsorption. Strong interaction between NH_3 or H_2O and the H^+ sites contained in H−Hol leads to a slow adsorption process. Time-courses of NH_3 adsorption show that NH_3 is adsorbed on the external surface or the tunnel entrance of H−Hol at first and then inserted into the inner part of the tunnel; the insertion stage is the more rate-determining process.

3. Adsorption and FT-IR results show that evacuation at a higher temperature leads to dehydration of physisorbed water in concurrence with a stepwise disappearance of proton sites on H−Hol. While one part of the dehydrated sites can become the dissociative sites for H_2O adsorption and recovered for NH_3 adsorption after rehydration, some proton sites are irreversibly lost due to surface rearrangement by valence change of Mn ions.

Acknowledgment. This work was supported by a Grant-in-Aid for Scientific Research from the special Coordination Fund (Frontier Ceramics Project) of the Science and Technology Agency of Japan.

CM0007609